Using the Quartz Crystal Microbalance with Dissipation Monitoring to Evaluate the Size of Nanoparticles Deposited on Surfaces

Adam L. J. Olsson, Ivan R. Quevedo, Danqing He, Mohan Basnet, and Nathalie Tufenkji*

Department of Chemical Engineering, McGill University, Montreal, Quebec H3A 2B2, Canada

ABSTRACT A quartz crystal microbalance with dissipation (QCM-D) monitoring can be an alternative tool to characterize nanoparticle size by virtue of its acoustic principle to sense adsorbed mass. In this study, sizes obtained by QCM-D for polymer-coated metallic nanoparticles and polydisperse polystyrene latex particle suspensions were compared with those obtained by transmission electron microscopy (TEM) and dynamic light scattering (DLS). We describe the obtained "QCM-D mass", which is weighted over surface area, by a general particle height distribution equation that can be used to determine the average particle diameter of a distribution of particles deposited on the QCM-D surface. Because the particle height distribution equation can be used for any particle geometry and surface packing geometry, it is described how the QCM-D can also be used to study the orientation of deposited nonspherical particles. Herein, the mean nanoparticle sizes obtained by QCM-D were generally in closer agreement with the primary particle size determined by TEM than with the sizes obtained by DLS, suggesting that primarily smaller particles within the particle population deposited on the sensor surface. Overall, the results from this study demonstrate that QCM-D could serve as an alternative and/or complementary means to characterize the size of nanoparticles deposited on a surface from suspensions of varying complexity.

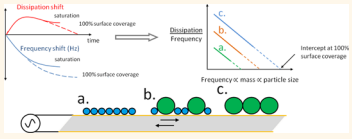

KEYWORDS: QCM-D · characterization · attachment · adsorption · particle · interfaces · mass transport

Nanoparticles display an exceptionally high surface area to volume ratio, which is being exploited in various science and engineering disciplines. In biomedical applications, for instance, liposomes/micelles and polymeric particles are used as carriers for drug delivery applications,[1] quantum dots (QDs) exhibit fluorescent properties, which makes them attractive for imaging applications,[2] and silver nanoparticles have been proposed as potential antimicrobial agents.[3] In environmental applications, highly reactive nanoparticles such as zerovalent iron (nZVI) are considered promising *in situ* remediation agents to transform chlorinated hydrocarbons and other environmental contaminants into innocuous products.[4,5] Nanoparticles can also be used as reactor catalysts (*e.g.*, silica-supported copper nanoparticles in methanol synthesis).[6]

As the particle size determines the surface area to volume ratio, thorough size characterization of nanoparticles is essential yet a major challenge. There are many nanoparticle sizing techniques available for nanoparticle suspensions. The commonly utilized dynamic light scattering (DLS) and nanoparticle tracking analysis (NTA) are simple to use and relatively cost efficient. However, because the intensity of the scattered light scales with the particle diameter raised to the sixth power, aggregates within polydisperse particle suspensions lead to a significant overestimation of the particle size.[7,8] Other more direct methods for visualizing the particles, such as transmission electron microscopy (TEM) and scanning electron microscopy (SEM), yield particle sizes (often in the dry state) but may suffer from subjective observational biases, and, furthermore, measurements involve sample preparation that is potentially intrusive.[7,8] Atomic force microscopy (AFM) can be used to determine the size of particles by scanning a surface coated with the target sample with a fine cantilever tip, but the analysis requires firmly attached particles to ensure that the tip itself does not manipulate the sample by, for instance, detaching the nanoparticles due to the applied force.[7−9] These are only a few examples of the

* Address correspondence to nathalie.tufenkji@mcgill.ca.

Received for review June 1, 2013 and accepted August 12, 2013.

Published online August 21, 2013
10.1021/nn402758w

advantages and limitations of selected sizing methods, and for a more detailed discussion on the subject we direct the reader to a recent review.[10] Simply put though, due to the limitations of each individual technique, accurate characterization of nanoparticle size is a nontrivial exercise. The method of choice should be carefully considered depending on sample type and experimental conditions; often, an array of characterization methods is required to corroborate the nanoparticle size.[7] Given the challenges associated with nanoparticle characterization, new analytical methods, preferably free from artifacts, are always of interest.

It was recently shown that data obtained from a quartz crystal microbalance (QCM) can be used to determine the size of particles deposited on a surface.[11] As the name implies, the QCM is a sensor of mass. The mass sensor as such consists of an AT-cut quartz crystal that, while driven by an AC current, oscillates at its fundamental and at its overtone resonance frequencies. Mass depositing onto the sensor surface is detected in real time as negative frequency shifts. Dissipative energy losses induced by the deposited masses are deduced from the oscillation decay time (*i.e.*, the so-called dissipation factor, D) or from the width of the oscillation peak (*i.e.*, half-bandwidth at half-maximum, Γ). These two factors are related *via*[12]

$$2\Gamma = Df_n \quad (1)$$

where f_n is the quartz crystal resonance frequency at the nth overtone. In the simplest of cases, when the adsorption forms a rigid and homogeneous film and the dissipative energy losses are small ($\Delta D_n/(\Delta f_n/n) < 10^{-7}$ Hz^{-1}), the adsorbed mass Δm is linearly proportional to the induced frequency shift according to the Sauerbrey relation:[13]

$$\Delta m = -\frac{\Delta f_n}{n} \times C \quad (2)$$

where Δf_n is the measured shift in QCM resonance frequency at overtone number n and C is the mass sensitivity constant that, for a 5 MHz AT-cut quartz crystal, equals 17.7 ng cm^{-2} Hz^{-1}. Note that standard software settings in QCM-D devices from Q-Sense provide the user with frequency shifts that are already normalized with respect to overtone number n. Because Sauerbrey's relation provides adsorbed mass in terms of ng/cm^2, simple division by the density of the depositing material yields an average film thickness (we henceforth refer to the outcome of these calculations as "Sauerbrey mass" and "Sauerbrey thickness", respectively).

Dissipative energy losses have been traditionally ascribed to an insufficient mass coupling of a viscoelastic film, whereupon the Sauerbrey relation underestimates the adsorbed mass (a.k.a. "the missing mass effect").[14,15] Importantly though, as pointed out in a recent review by Reviakine *et al.*,[12] the underlying assumption for the viscoelastic model to apply is that the mass deposits as a homogeneous film and *not* as discrete elements, as in the case of nanoparticle deposition. Rather, it has been demonstrated by finite element modeling (FEM) that, in the case of discrete objects, the dissipative energy losses originate from the boundary between the particle and an *a priori* unknown amount of liquid that is being dragged by the particle (referred to as hydration coat)[16,17] during crystal oscillation[18] and, furthermore, is dependent on the stiffness of the particle−surface bond. During particle deposition, the fractional amount of liquid within the heterogeneous film, and therewith the dissipative energy losses, decrease with particle surface coverage.[16,17] Tellechea *et al.*[11] further demonstrated that when plotting the shifts in dissipative energy losses (either ΔD or $\Delta\Gamma$) over frequency shift as a function of the normalized frequency shift (*i.e.*, $\Delta D_n/\Delta f_n$ or $\Delta\Gamma_n/\Delta f_n$ *vs* $\Delta f_n/n$), extrapolation of a linear regression fit reveals an intercept of $\Delta f_n/n$ for a hypothetical 100% surface coverage, where the fractional trapped liquid has diminished to occupy only the void spaces between densely packed particles (see Supporting Information, Figure S1, for a descriptive schematic depiction of this analysis). Because the intercept occurs when dissipative energy losses approach zero, Sauerbrey's relation applies. The Sauerbrey mass divided by the particle density yields a Sauerbrey thickness that effectively corresponds to the mean particle diameter.[11] Dultsev and co-workers have suggested another interesting approach to determine the size distribution of particles deposited on surfaces using QCM.[19] In their approach, the QCM sensor acts as a microphone by which one "listens" to the noise generated by the rupture of particle−surface bonds as the oscillation amplitude is gradually elevated by increased drive voltage. It is proposed that the bonds rupture when the inertial force of the particles in movement exceeds the force of attachment. Under the assumption that the attachment force scales with the contact area (which in turn scales with the particle radius), a distribution of numbers proportional to particle sizes is generated. This approach requires that the crystal drive amplitude is tunable in a very controlled manner that is not yet possible in commercially available QCMs. Furthermore, because the approach relies on detachment of particles, converting these numbers to real particle size requires knowledge of the attachment force.

The method proposed by Tellechea *et al.*[11] derives the particle size microgravimetrically and, therefore, does not rely on bond rupture due to increased oscillation amplitudes, which makes the analysis straightforward to implement in commercially available QCM-D without prior knowledge of the adhesive force. The method requires no specific sample preparation, and the particle size is derived *in situ*. This brings another interesting aspect in the context of, for example, nanoparticle transport in environmental systems or filtration,[20−24]

in that particle deposition kinetics and particle size can be determined within the same experiment.

To date, the method has been applied to determine the diameter of monodisperse samples of adhering cowpea mosaic viruses and liposomes[11] and to study the deformation of liposomes adhering to titanium dioxide surfaces at different temperatures.[25] Herein, we demonstrate how the method can be used to determine the size of deposited particles of more complex particle suspensions, namely, polydisperse suspensions and suspensions of surface-modified nanoparticles. The aim is to identify potential biases caused by, for instance, preferential adsorption of different size classes within a distribution. We also investigate whether the force of attachment is crucial for the outcome of the measurements by performing experiments on negatively and positively charged surfaces. We demonstrate that (i) the method provides an "apparent" particle size that scales with the particle height (or diameter for spherical particles) and that (ii) can be described by a generalized expression of the particle size distribution on the surface, and (iii) unless the deposited particles are firmly attached to the surface, they slip, and the method may underestimate the particle size.

RESULTS

QCM-D Sizing of Carboxylated Polystyrene Latex Particles. Figure 1a,b and Figure 1d,e present the frequency shifts and dissipation shifts caused by deposition of the different polystyrene latex particle suspensions onto alumina- (upper panels) and silica-coated (lower panels) QCM-D sensor surfaces. On the positively charged alumina surface (alumina is positively charged below pH 9),[26] the monodisperse 24 nm particle suspension deposited at the fastest rate and exhibited the smallest frequency shift (~80 Hz) and the smallest dissipation shift ($\sim 2 \times 10^{-6}$) at saturation. The monodisperse 110 nm particle suspension deposited the slowest but exhibited the largest frequency shift (~270 Hz) and the largest dissipation shifts ($\sim 25 \times 10^{-6}$) at saturation. The 50/50 and the 25/75 mixtures (m_{24nm}/m_{110nm}) deposited at intermediate average rates, reaching frequency shifts and dissipation shifts of intermediate levels at saturation (~100−135 Hz and $\sim(2.5-10) \times 10^{-6}$, respectively). Similar trends were observed on negatively charged silica, although the frequency shifts at saturation were all considerably lower than on alumina and the deposition rates were slower.

Figure 1c and f present the corresponding $\Delta D_n/(\Delta f_n/n)$ *vs* $\Delta f_n/n$ plots and the extrapolation of linear regression analyses for determining the value of $\Delta f_n/n$ at the intercept for the different polystyrene latex particle suspensions depositing onto alumina and silica, respectively. On both the alumina and the silica surfaces, the intercept gradually shifted toward larger $\Delta f_n/n$ values as the concentration of the 24 nm *c*PL particle decreased and the concentration of the 110 nm *c*PL particle increased. Comparing the data sets from the two different surfaces reveals two notable features: (i) the $\Delta f_n/n$ intercept values were larger on alumina than on silica and (ii) the $\Delta D_n/(\Delta f_n/n)$ values were lower on alumina than on silica. The corresponding Sauerbrey thicknesses for each suspension (using a particle density ρ = 1.05 g/cm^3) on both surfaces are listed in Table 1 together with their corresponding size class ratios (based on mass), number-averaged nominal sizes (calculated from known particle nominal sizes and known mass concentrations), electrophoretic mobilities, and hydrodynamic diameters (*Z*-, number-, and intensity-averages). On alumina, the Sauerbrey thicknesses obtained for the monodisperse suspensions (24 ± 2 and 114 ± 6 nm) were very similar to the reported nominal sizes (24 and 110 nm, respectively). For the bimodal suspensions, the Sauerbrey thicknesses were substantially larger (38 ± 9 and 59 ± 10 nm) than the average nominal sizes (25 and 26 nm, respectively). On silica, the Sauerbrey thicknesses were all thinner (12 ± 3, 16 ± 4, 17 ± 7, and 80 ± 29 nm) than the corresponding calculated number averages (24, 25, 26, and 110 nm, respectively). In DLS, the corresponding *Z*-averages were 72 ± 2, 108 ± 3, 113 ± 1, and 114 ± 1 nm; the corresponding number-averages were 23 ± 1, 79 ± 5, 85 ± 7, and 93 ± 4 nm; and the corresponding intensity-averages were 184 ± 62, 119 ± 3, 123 ± 3, and 121 ± 2 nm, respectively.

QCM-D Sizing of Surface-Modified Palladium-Doped nZVI (Pd-nZVI). Figure 2 presents the average frequency shifts (a) and average dissipation shifts (b) caused by Pd-nZVI particle deposition on silica for particles whose surfaces had been modified with either 90 or 700 kDa carboxymethyl cellulose (CMC). The maximum deposition rates as well as the total frequency shift and the total dissipation shift at saturation were larger for the 90 kDa CMC-coated Pd-nZVI particles than for the 700 kDa CMC-coated Pd-nZVI particles. The corresponding $\Delta D_n/(\Delta f_n/n)$ *vs* $\Delta f_n/n$ plots can be presented for only two measurements of the 90 kDa CMC-coated particles (Figure 2c), while for the other measurements, the extent of deposition was too low to obtain the linear segment of the $\Delta D_n/(\Delta f_n/n)$ *vs* $\Delta f_n/n$ curve required for extrapolation. The $\Delta f_n/n$ intercepts for the 90 kDa CMC-coated particles were found to be on the order of 1000 Hz, which corresponds to a Sauerbrey thickness of approximately 45 nm (using a particle density ρ = 5 g/cm^3).[27] In DLS, the *Z*-averages were 957 ± 44 and 428 ± 20 nm; the number-averages were 384 ± 133 and 163 ± 19 nm; and the intensity-averages were 1622 ± 210 and 783 ± 80 nm, for the 90 kDa CMC-coated Pd-nZVI particles, respectively (Table 2). TEM image analysis revealed nominal particle sizes below 50 nm and average aggregate sizes

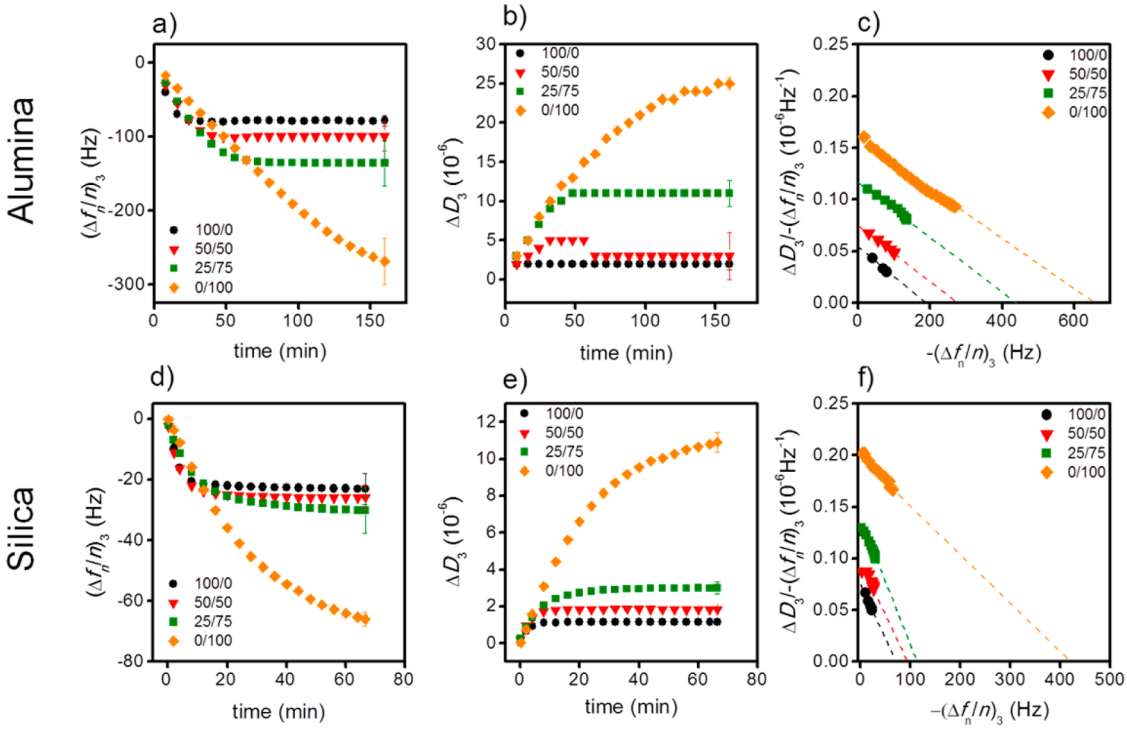

Figure 1. Average normalized frequency shifts ($\Delta f_n/n$) and dissipation shifts (ΔD_n) of the third overtone as a function of time during polystyrene latex nanoparticle deposition for nanoparticle suspensions of different mass ratios (m_{24nm}/m_{110nm}) on alumina (a and b) and on silica (d and e) and the corresponding $\Delta D_n/-(\Delta f_n/n)$ *vs* $\Delta f_n/n$ plots (c and f, respectively). Data are presented as averaged values, and error bars represent SD over three independent measurements. Linear regression analysis yields $\Delta f_n/n$ intercepts for hypothetical 100% surface coverage scenarios that are converted into Sauerbrey thickness (presented in Table 1).

TABLE 1. Mass Ratios, Number-Averaged Particle Sizes, Electrophoretic Mobilities, DLS Hydrodynamic Diameters (*Z*-, Number-, and Intensity-Averages), Polydispersity Indexes (PDI), and Sauerbrey Thicknesses on Silica and Alumina Surfaces of the Four Different Carboxylated Polystyrene Latex Mixtures

				DLS				QCM-D		
		number-average	electrophoretic mobility	*Z*-average	intensity-average	number-average		Sauerbrey thickness (nm)[a]		
particle	mass ratio m_{24}/m_{110}	(nm)	(μm cm/V sec)	(nm)	(nm)	(nm)	PDI[b]	silica	alumina	S.L. prediction[c]
carboxylated polystyrene latex	100/0	24	-2.7 ± 0.1	72 ± 2	203 ± 62	23 ± 1	0.4	12 ± 3	24 ± 2	24
	50/50	25[d]	-2.3 ± 0.1	108 ± 3	119 ± 3	79 ± 5	0.1	16 ± 4	38 ± 9	39
	25/75	26[d]	-2.2 ± 0.1	113 ± 1	123 ± 3	85 ± 7	0.1	17 ± 7	59 ± 10	60
	0/100	110	-2.1 ± 0.1	114 ± 1	121 ± 2	93 ± 4	0.1	80 ± 29	114 ± 6	110

[a] Sauerbrey thickness is calculated from the Sauerbrey mass at hypothetical 100% surface coverage. [b] PDI = polydispersity index. [c] S.L. predictions (last column) are the calculated Sauerbrey thicknesses, using eq 8 and the particle deposition rate based on the Smoluchowski–Levich approximation. [d] Values calculated from the known nominal sizes and the mass ratios indicated for each suspension.

of 126 ± 49 nm for the 90 kDa CMC-coated Pd-nZVI particles (Figure S2a and b and Table 2).

QCM-D Sizing of CdSe and CdTe QDs. The measurements of QD deposition onto alumina using QCM-D have been published elsewhere[24] and reanalyzed here according to the approach proposed by Tellechea *et al.*[11] The particles were deposited onto positively charged alumina (at pH 5) at different solution ionic strength (IS). Representative frequency and dissipation shifts and the corresponding $\Delta D_n/(\Delta f_n/n)$ *vs* $\Delta f_n/n$ plots of the third overtone for the CdSe QD and the CdTe QD are included in Figure 2d–f and g–i, respectively. For the CdSe QD, the deposition rate as well as the total frequency and dissipation shifts at saturation increased as the salt concentration in solution decreased. For the CdTe QD, the opposite trend was observed. We have previously explained this behavior in terms of collapse of the CdTe QD's sterically stabilizing polyelectrolyte coating.[23] In DLS, for the CdSe QD, the *Z*-averages were 175 ± 49, 193 ± 108, and 565 ± 113 nm;

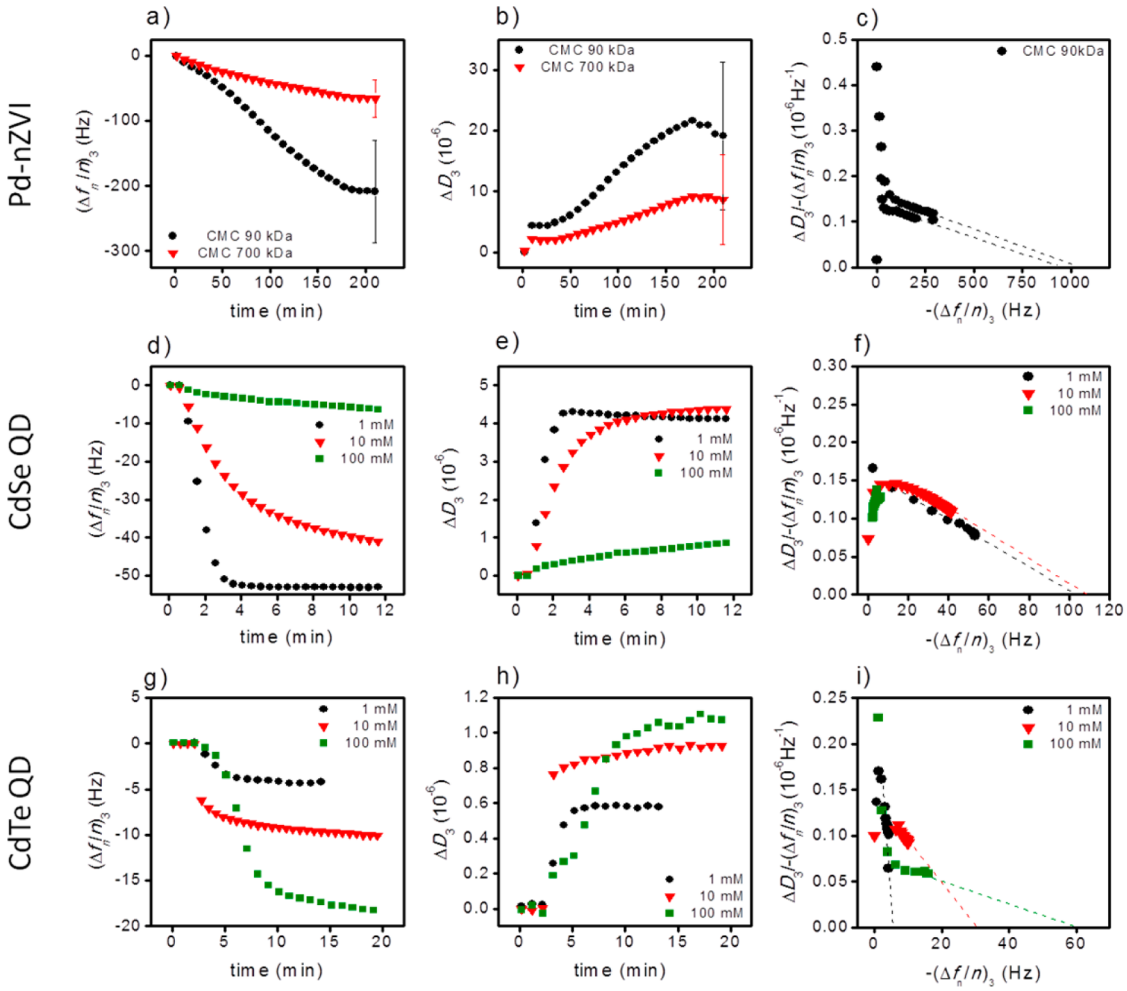

Figure 2. Normalized frequency shifts ($\Delta f_n/n$) and dissipation shifts (ΔD_n) of the third overtone as a function of time during nZVI deposition onto silica (a and b) and CdSe QD and CdTe QD deposition onto alumina (d, e and g, h) and the corresponding $\Delta D_n/-(\Delta f_n/n)$ *vs* $\Delta f_n/n$ plots (c, f, and i, respectively). In a and b, the error bars represent SD over three independent measurements, whereas in c and f each curve is one representative measurement from previously published data. Linear regression analysis yields $\Delta f_n/n$ intercepts for hypothetical 100% surface coverage scenarios that are converted into Sauerbrey thickness (presented in Table 2).

TABLE 2. Electrophoretic Mobilities, DLS Hydrodynamic Diameters (Z-, Number-, and Intensity Averages), Polydispersity Indexes (PDI), TEM Aggregate and Primary Particle Sizes, and Sauerbrey Thicknesses of Pd-nZVI, CdSe QD, and CdTe QD

					DLS				TEM		QCM-D
particle	electrolyte	coating	ionic strength (mM)	electrophoretic mobility (μm cm/V sec)	*Z*-average (nm)	number-average (nm)	intensity-average (nm)	PDI[b]	aggregate size (nm)	particle size (nm)	Sauerbrey thickness[a] (nm)
Pd-nZVI	$NaHCO_3$	CMC-90 kDa	3	-4.1 ± 0.1	957 ± 44	384 ± 133	1622 ± 210	0.5	126 ± 49	<50	~45
		CMC-700 kDa	3	-5.0 ± 0.0	428 ± 20	163 ± 19	732 ± 80	0.5			n.d.[c]
CdSe QD	KCl	poly ethylene-glycol (PEG)	1	-1.6 ± 0.0	196 ± 68	58 ± 48	408 ± 227	0.4	30 ± 20	~5	8 ± 3
			10	-0.7 ± 0.1	244 ± 26	19 ± 7	349 ± 120	0.7			9 ± 0
			100	-0.3 ± 0.1	257 ± 30	203 ± 34	384 ± 28	0.3	68 ± 66	~5	10 ± 5
CdTe QD	KCl	polyacrylic-acid (PAA)	1	-1.8 ± 0.0	59 ± 4	6 ± 3	73 ± 14	0.2	29 ± 4	~5	1 ± 0
			10	-1.9 ± 0.0	88 ± 19	12 ± 12	134 ± 54	0.4			3 ± 0
			100	-1.8 ± 0.1	192 ± 3	117 ± 15	305 ± 9	0.2	67 ± 46	~5	4 ± 1

[a] Sauerbrey thickness is calculated from the Sauerbrey mass at hypothetical 100% surface coverage. [b] PDI = polydispersity index. [c] n.d. = the value could not be determined because too few particles deposited on the QCM surface.

the number-averages were 58 ± 48, 19 ± 17, and 203 ± 34 nm; and the intensity-averages were 408 ± 227, 349 ± 120, and 384 ± 28 nm at 1, 10, and 100 mM KCl, respectively. For the CdTe QD, the *Z*-averages were 59 ± 4, 88 ± 19, and 117 ± 15 nm; the number-averages were 6 ± 3, 12 ± 12, and 117 ± 15 nm; and the intensity averages were 73 ± 14, 134 ± 54, and 305 ± 9 nm at 1, 10, and 100 mM KCl, respectively. The QCM analysis described herein yielded equivalent Sauerbrey thicknesses (using particle density ρ = 2.4 g/cm^3)[24] of 8 ± 3, 9 ± 0, and 10 ± 5 nm for the CdSe QD and 1 ± 0, 3 ± 0, and 4 ± 1 nm for the CdTe QD at 1, 10, and 100 mM KCl, respectively. Inspection of the corresponding TEM images (Figure S2c,d and e,f) revealed larger nanoparticle aggregates (on the order of 20−100 nm) composed of clearly visible QDs with a size of a few nanometers.

DISCUSSION

Herein, we have investigated the versatility of a QCM-D to determine the size of engineered nanoparticles in suspensions of varying complexity. We first turn our discussion toward the effect of sample polydispersity. In Figure 1c,f, it is evident that the $\Delta f_n/n$ at the intercept increased as the relative ratio between small (24 nm) and large particles (110 nm) decreased. This was the case on both positively charged alumina and negatively charged silica, which is an expected result since a larger average particle size should in theory add more mass to the sensor surface than smaller particles. For the monodisperse suspensions, when the $\Delta f_n/n$ intercept values are converted to Sauerbrey mass, and further converted into Sauerbrey thickness, it appears that the QCM-D yields particle sizes within a few nanometers of the nominal size for both particles on alumina. In contrast, on silica, the particle sizes obtained from the QCM-D measurements were only ∼1/2 to ∼3/4 of the nominal values. Tellechea *et al.*[11] reported particle sizes obtained by QCM that corresponded within a few nanometers of the particle sizes obtained by DLS (*Z*-average) for mosaic pea viruses adhering to Au-coated surfaces and liposomes adhering to TiO_2-coated surfaces. Herein, for the monodisperse suspension of the small particle, particle size obtained by DLS varied depending on whether one considers Z-, number-, or intensity-based averages, suggesting a certain degree of aggregation within the sample. However, because the number-average was close to the reported nominal size, we expect most particles to be present as individuals in suspension, and we can calculate a number-averaged particle size (Table 1).

When comparing to the calculated number-average, it appears that QCM-D overestimated the particle size when the mixed suspensions were analyzed following deposition on alumina. It is important to note that QCM-D measures the average size of the *deposited* particles, which does not necessarily correspond with the average particle size in suspension. It is unlikely, however, that the overestimation of particle size seen herein is due to deposition of a greater fraction of the larger 110 nm particle to the sensor surface than the smaller 24 nm particle. This is because the smaller particle should deposit more due to more rapid diffusion to the surface and, additionally, the smaller particle is more negatively charged (Table 1), which would further favor deposition on the positively charged alumina surface.

To better understand this overestimation of the particle size, one has to take into account that the Sauerbrey mass, which is defined as area-averaged mass per unit area (ng/cm^2), is derived from the area-averaged stress−speed ratio at the crystal surface.[28] Whereas the average speed within an oscillation cycle can be considered constant, the stress is proportional to the sample's inertia (*i.e.*, mass) but inversely proportional to the sample−surface contact area. For continuous and homogeneous films, the sample−surface contact area equals the sensor surface area, and variations in Sauerbrey mass are determined by film density and thickness alone. The stress contribution of individual objects within a discrete film, however, depends on their mass−contact area ratio and, thus, also on particle geometry, size, and orientation. In other words, the mass contribution to the total Sauerbrey mass of any individual object within a discrete film must be defined by its mass weighted over the surface area that it occupies on the sensor surface. Here, we treat the deposited film (at 100% surface coverage) as hexagonally close-packed spheres and define an individual particle's Sauerbrey mass (*i.e.*, the mass per unit area) as

$$m_{\text{Sauerbrey}} = \frac{h2a^2\sqrt{3}\rho}{2a^2\sqrt{3}} = h\rho \qquad (3)$$

where a is the apothem and h is the height of the hexagonal prism, respectively, which are equivalent to the radius and the diameter of the deposited particle, respectively. ρ is the hexagonal prism's average density, which can be calculated by

$$\rho = \phi_p\rho_p + \phi_s\rho_s \qquad (4)$$

where ϕ_p and ϕ_s are the volume fractions of the particle and the solvent (in this case water), which for the hexagonal geometry described in eq 3 equal 0.6 and 0.4, respectively (for details, see Supporting Information, Figure S2). Equation 3 describes the Sauerbrey mass of hexagonally close-packed spheres but can, in principle, be rewritten for particles of any geometry and/or surface orientation.

Defining the Sauerbrey mass for individual particles is of little or no importance when interrogating monodisperse samples. Because all particles are of the same volume, they contribute equally to the total Sauerbrey mass and form a homogeneous layer at 100% surface

coverage; hence, the Sauerbrey thickness corresponds to the average particle height.[11] Within polydisperse suspensions, however, because the particle's individual Sauerbrey mass scales with its height eq 3, larger particles skew the Sauerbrey mass toward larger values. Consequently, the Sauerbrey thickness will correspond to an overestimated "apparent" particle height (h_{app}) that can be defined as

$$h_{app} = \frac{M_{Sauerbrey}}{\rho} \quad (5)$$

where $M_{Sauerbrey}$, which is the total Sauerbrey mass calculated from the $\Delta f_n/n$ intercept, is a function of the particle height (size) distribution and is described by the general expression

$$M_{Sauerbrey} = \frac{\rho \sum_{i=1}^{n} m_i h_i}{\sum_{i=1}^{n} m_i} \quad (6)$$

where m_i and h_i are the mass and height, respectively, of each size class within the population.

For a bimodal distribution, as investigated herein, eq 6 takes the form of

$$M_{Sauerbrey} = \rho\left(\frac{m_s h_s + m_l h_l}{m_s + m_l}\right) \quad (7)$$

where m_s and m_l are the masses and h_s and h_l are the heights of the small and large particles, respectively. The expression can be further simplified to

$$M_{Sauerbrey} = \rho(\theta_s h_s + (1 - \theta_s)h_l) \quad (8)$$

where θ_s is the ratio (by mass) of the small to the total amount of particles on the surface.

We have used eq 8 to calculate the contribution of small particles (θ_s) to the total Sauerbrey mass ($M_{Sauerbrey}$) calculated from the $\Delta f/n$ intercept obtained from experiments (Figure 1c). We arrived at θ_s = 84% for the 50/50 mixture and at θ_s = 59% for the 25/75 mixture. Qualitatively, this reflects well the difference in the convective−diffusive transport of the two size classes that one would expect; that is, the smaller particle diffuses faster and therefore deposits at a higher rate. For a more quantitative comparison, we adopted the so-called Smoluchowski−Levich approximation to calculate theoretical particle deposition rates for each size class, under the assumption that the mass transport is purely convective−diffusive.[24,29] The calculated theoretical mass deposition rates of the small particle amounted to 83% and 58% of the total mass deposition rate for the 50/50 and the 25/75 mixture, respectively. These values are very close to the particle distribution on the surface as calculated from the Sauerbrey mass using eq 8, providing further support of the model. Alternatively, eqs 8 and 5 can be used to predict an apparent Sauerbrey thickness h_{app} using the theoretical deposition rates of the two size classes obtained from the Smoluchowski−Levich approximation. When θ_s equaled 0.83 and 0.58, the Sauerbrey thickness h_{app} was calculated to be 39 and 60 nm, respectively, which is in close agreement with the experimentally obtained values (Table 1, last column).

Equations 3−8 describe how the Sauerbrey mass/thickness is dependent on the particle distribution on the surface, which in turn is dependent on the deposition rate of each size class within the suspended population. On alumina, the particle distribution is governed by convective−diffusive transport alone and the particle size distribution can be interpreted in terms of the Smoluchowski−Levich approximation. On silica, however, because both the surface and the particles are negatively charged, the deposition is affected also by electrostatic repulsion. Considering that the magnitude of electrostatic repulsion scales with the particle size,[30,31] it is expected that the larger particle deposits at a lower rate, yielding Sauerbrey thicknesses that are closer to the nominal size (and number-sized distribution in DLS) of the smaller particle than the larger particle for the polydisperse mixtures of polystyrene latex particles.

The presence of electrostatic repulsion has another significant effect on the experimental outcome in that the particle sizes are underestimated by as much as half of the nominal sizes for the monodisperse suspensions. This phenomenon can be ascribed to differences in the adhesive bond properties. As has been previously demonstrated using FEM analysis, the magnitude of $\Delta D_n/(\Delta f_n/n)$ decreases with the stiffness of the bond between the particle and the sensor surface,[18] and the decreasing bond stiffness eventually results in particle slip (*i.e.*, the particle no longer moves in unison with oscillation of the sensor surface).[18] By applying a coupled resonance model, Olsson *et al.* showed that the stiffness of the bonds between micrometer-sized silica particles and bare silica surface increases with IS due to reduced electrostatic repulsion.[32] The authors also acknowledged that a dimensionless coupling factor (termed oscillator strength, f_{osc}), ranging from "not coupled" (f_{osc} = 0) to "fully coupled" (f_{osc} = 1), was necessary to model their data.[32] Thus, it is likely that the steeper slope of $\Delta D_n/(\Delta f_n/n)$ *vs* $\Delta f_n/n$ observed when going from attractive electrostatic conditions on positively charged alumina to repulsive electrostatic forces on negatively charged silica (compare Figure 1c with f) reflects a decrease in bond stiffness, which in turn causes the particle mass to not fully couple to the oscillation of the sensor surface (*i.e.*, particle slip), whereupon the value of the $\Delta f_n/n$ intercept decreases and the Sauerbrey mass/thickness is underestimated. This is a significant finding because it suggests that the accuracy of the nanoparticle sizing analysis is dependent on firm attachment of the particles to the sensor

surface. Depending on the experimental conditions (*e.g.*, different ionic strength and pH), the adsorbed mass may be underestimated by the QCM-D. The above are important fundamental theoretical considerations that have implications for the general interpretation of nanoparticle deposition using QCM-D, *e.g.*, when particle attachment efficiencies are determined by normalizing measured nanoparticle deposition rates under unfavorable conditions (in the presence of repulsive energy barriers) to the deposition rates under favorable conditions (in the absence of repulsive energy barriers) determined either experimentally[20,21] or theoretically.[24,29]

Because many nanoparticles are coated with surface modifiers to achieve their desired functionality and to render them stable in aqueous suspension, we have also evaluated whether the method can be used to determine particle size for surface-modified nanoparticles by performing experiments with CMC-coated Pd-nZVI. When examining the kinetics of the frequency and dissipation shifts (Figure 2a and b), it became evident that the 700 kDa CMC coating is more effective in preventing Pd-nZVI nanoparticle deposition on silica than the 90 kDa CMC coating. The 700 kDa CMC coating was not only effective in preventing deposition but also better stabilized the particles, which is in agreement with an earlier study.[33] Inspection of DLS data (Table 2) reveals that Z-, intensity-, and number-average hydrodynamic diameters were all smaller for 700 kDa CMC-coated particles than the 90 kDa CMC-coated particles. Yet, the large variation between the Z-, intensity-, and number-averaged particle sizes, indicative of polydisperse suspensions, suggests that the particles are to some extent prone to aggregation in spite of their surface modification. The corresponding size obtained by the QCM-D sizing analysis for the particle coated with 90 kDa CMC was approximately 45 nm. Interestingly, this is in closer agreement with the primary particle size (*i.e.*, below 50 nm) than the average aggregate size (126 ± 49 nm) obtained from TEM images (Figure S2a and b) of the same particle (Table 2). Similar to the bimodal polystyrene latex suspension, this is linked to the fact that smaller particles within polydisperse suspensions diffuse toward the surface at a higher rate than larger particles and that the contribution of repulsive electrostatic interactions is less important for the smaller particles. It should be noted that for the Pd-nZVI particle the linear regression and extrapolation of the QCM-D data is less rigorous (*i.e.*, shorter linear segment of the $\Delta D_n/(\Delta f_n/n)$ *vs* $\Delta f_n/n$ plots) than for the polystyrene latex particles due to an overall lower extent of deposition of CMC-coated Pd-nZVI. The QCM-D analysis requires a surface coverage of approximately 10−20%, as it is under these conditions that the particles are close enough to one another to decrease $\Delta D_n/(\Delta f_n/n)$ by sharing their hydration coats,[34] which is a prerequisite for the analysis. This criterion is not always easily achieved, especially for electrosterically stabilized nanoparticles. In this case, for instance, only two out of three measurements for the 90 kDa CMC-coated particles exhibit sufficient surface coverage to allow for the analysis (Figure 2c), albeit still with rather poor accuracy. The magnitude of experimental error associated with low surface coverage is difficult to predict. For the polystyrene latex particles, low surface coverage on silica appears to cause larger standard deviations (∼25−40% of the mean) than high surface coverage on alumina (∼1−25% of the mean) (Table 1). However, this could also be an effect of particle slip. When the same particles were firmly attached, the largest variation was observed for the mixed suspensions, suggesting that the main source of error is from variation within the sample (Table 1). The need of sufficient surface coverage is clearly a limitation of the method, but it can potentially be circumvented by working with sensor surfaces that are charged oppositely of the particle to enable higher surface coverage (*e.g.*, compare polystyrene latex deposition on silica and alumina, Figure 1).

To investigate this further, we are also including previously published QCM-D deposition data obtained using other types of surface-modified nanoparticles, namely, CdSe and CdTe QDs depositing on alumina-coated sensor surfaces at different solution IS.[24] Representative QCM-D measurements for the CdSe and CdTe QDs at three different IS and the corresponding $\Delta D_n/(\Delta f_n/n)$ *vs* $\Delta f_n/n$ plots are presented in Figure 2d−f and g−i, respectively. As anticipated, particle deposition was higher and therefore the linear segment was longer when the negatively charged QDs deposited on the positively charged alumina surface, and thus, the $\Delta D_n/(\Delta f_n/n)$ *vs* $\Delta f_n/n$ extrapolation was more rigorous under these conditions. For both particles, the Sauerbrey thickness was in closer agreement with the diameter of individual particles observed (together with larger aggregates) in TEM images (Figure S3 and Table 2). In fact, the Sauerbrey thickness was fairly consistent with the primary particle size over the entire range of IS, even though the increasing salt concentration appeared to induce even more aggregation, leading to larger particle sizes measured by DLS. *Z*-, number-, and intensity-averaged particle sizes all suggested a similar trend (Table 2). Again, this indicates that although the samples are aggregating in suspension, large subpopulations of small nonaggregated particles are still dominating the deposition over the larger aggregates due to more rapid diffusion to the sensor surface.

CONCLUSIONS

Summarizing, a QCM-D was applied to investigate the size of engineered nanoparticles deposited onto

different surfaces from suspensions of varying complexity. The particle diameters were obtained by determining the average layer thickness of films composed of deposited nanoparticles on either silica- or alumina-coated QCM-D sensor crystals. The average layer thickness was determined from the Sauerbrey mass at a hypothetical 100% surface coverage by extrapolation of $\Delta D_n/(\Delta f_n/n)$ *vs* $\Delta f_n/n$ plots.[11] We have shown that the total Sauerbrey mass is given by the sum of all particles' masses weighted over the sum of the area they occupy on the sensor surface. Herein, all particles were treated as spheres depositing in a hexagonal close-packed geometry. This meant that the Sauerbrey mass scaled with the particle diameter, which caused the Sauerbrey thickness to be biased toward larger particles within a distribution. Importantly, the proposed equations can be rewritten for any other particle and/or packing geometry. This suggests that another interesting application for the method is the study of the orientation of nonspherical particles deposited on a sensor surface. If the size and geometry of nonspherical particles are known, then the Sauerbrey thickness is indicative of the particle orientation. These results demonstrate that QCM-D could serve as alternative and/or complementary means to characterize the size of nanoparticles deposited on different surfaces from suspensions of varying complexity. However, we found that this method requires relatively high surface coverage, which, depending on the experimental conditions, is not always easily achieved. This was especially true when particles were deposited onto like-charged surfaces. Not only was the deposition low for rigorous extrapolation of the $\Delta D_n/(\Delta f_n/n)$ *vs* $\Delta f_n/n$ plots, the layer thickness was also underestimated by as much as half of the particle diameter. This observation could be ascribed to insufficient coupling of the nanoparticle to the surface under unfavorable deposition conditions (in the presence of electrostatic repulsion between the particles and the sensor), which causes the particles to "slip" on the sensor surface.[18] For the first time, it was experimentally shown that the slope of the $\Delta D_n/(\Delta f_n/n)$ *vs* $\Delta f_n/n$ plots, which is dependent on the stiffness of the particle−surface bond, is influenced by surface charge. Thus, this study also demonstrates that, in addition to determining the particle size, the method can be used to study the mechanical properties of the particle−surface adhesive bonds.

METHODS

Preparation of ENP Suspensions. *Carboxyl-Functionalized Nanoparticles.* Carboxyl-modified polystyrene latex nanospheres (Invitrogen), with reported nominal sizes of 24 and 110 nm (according to the vendor), were used to prepare nanoparticle suspensions at 10 mM KCl (pH 4). Two monodisperse suspensions were prepared by suspending each particle to a final mass concentration of 4.4×10^6 μg/mL, corresponding to 10^{12} and 8×10^9 particles/mL for the 24 nm and the 110 nm, respectively. Two bimodal suspensions, of either 50/50 or 25/75 mass to mass ratio (m_{24nm}/m_{110nm}), were also prepared. The 50/50 (m_{24nm}/m_{110nm}) suspension was prepared by suspending 2.2×10^6 μg/mL of each particle into the same suspension, which corresponds to 5×10^{11} and 4×10^9 particles/mL for the 24 nm and the 110 nm particle, respectively, and an average particle diameter of 25 nm. The 25/75 (m_{24nm}/m_{110nm}) suspension was prepared by suspending 1.1×10^6 μg/mL of the 24 nm particle and 3.3×10^6 μg/mL of the large, 110 nm particle into the same suspension, which corresponds to 2.5×10^{11} and 6×10^9 particles/mL for the 24 nm and the 110 nm particle, respectively, and an average particle diameter of 26 nm. To assess the average Sauerbrey thickness from the Sauerbrey mass, we used a polystyrene latex particle density of 1.05 g/cm^3.

Palladium-Doped Nanosized Zerovalent Iron (Pd-nZVI) Particles. Stock slurry of bare nZVI was obtained from Golder Associates Inc. (Montreal, Canada), vacuum-dried, and stored in a N_2-purged hypoxic chamber. The nZVI stock suspension (10 g/L) was prepared by suspending the dried nZVI powder in N_2-purged deionized (DI) water and ultrasonicating for 20 min (Misonix sonicator, S-4000). The nZVI surface was doped with palladium by soaking in an ethanol solution of palladium acetate (Sigma). The ratio of palladium acetate to nZVI mass was 0.01 (w/w %). The stock Pd-nZVI suspension was stored in a N_2-purged hypoxic chamber until further use. For each experiment, the working suspension was prepared by diluting the stock in DI water, probe ultrasonicating for 10 min, and immediately mixing with a carboxymethyl cellulose (Sigma) solution followed by gentle mixing for 1 h using a 360° rotator (Lab Revolution, Mandel). The final Pd-nZVI concentration was 150 mg/L, and the Pd-nZVI to CMC mass ratio was 0.4. The solution ionic strength was adjusted to 3 mM by adding $NaHCO_3$, and the pH was adjusted to 7.7 by addition of HCl. To assess the average Sauerbrey thickness from the Sauerbrey mass, we used a Pd-nZVI particle density of 5 g/cm^3.[27]

Carboxyl-Terminated QDs. Details on the preparation of QD suspensions and the QD deposition experiments have been published elsewhere;[24] however, the QCM-D data are reanalyzed here according to the approach described by Tellechea *et al.*[11] In brief, the particle suspensions were prepared as follows: polyacrylic-acid (PAA)-stabilized CdTe/CdS QDs (Vive Crop Protection, catalog no. 18010 L) and poly(ethylene glycol) (PEG)-coated CdSe/ZnS QDs (T2 MP-Evitags, from Evident Technologies) were suspended in KCl at 1, 10, and 100 mM to final concentrations of 2×10^{13} particles/mL and an adjusted pH of 5 (using HCl). The QD suspensions were stored overnight at 9 °C prior to each QCM-D experiment. To assess the average Sauerbrey thickness from the Sauerbrey mass, we used CdSe and CdTe particle densities of 2.4 g/cm^3.[23]

Particle Characterization. *Particle Size.* The nominal particle sizes reported by the vendors were 10 nm for the CdTe QD, 25 nm for the CdSe QD, and 24 and 110 nm for the two *c*PL nanoparticles. The nominal sizes of the QDs and the Pd-nZVI were evaluated by transmission electron microscopy for selected conditions (Phillips CM200), using protocols described elsewhere.[35] Representative TEM images for Pd-nZVI, CdSe, and CdTe QDs are presented in the Supporting Information (Figure S3). Hydrodynamic diameters (*i.e.*, particle size) and polydispersity index (PDI) of the different nanoparticles were determined by DLS (ZetaSizer Nano, Malvern) using at least three different samples of each suspension.

Electrokinetic Properties. The electrophoretic mobility of the nanoparticles at different IS was determined by measuring the velocity of the particles *via* laser Doppler velocimetry (ZetaSizer Nano ZS, Malvern). Each measurement was performed in triplicate using disposable capillary cells with an adjusted electrical field (E) between 5 and 10 ± 0.1 V/m.

QCM-D Measurements. Nanoparticle deposition rates on Al_2O_3 (alumina) and SiO_2 (silica) coated QCM sensors (QSX-309 and QSX-303, Q-Sense AB, Gothenburg, Sweden) were measured using a QCM-D E4 setup (Q-Sense AB). The QCM-D measurements were performed as follows. First, particle-free electrolyte was allowed to flow through the QCM-D chamber until both Δf and ΔD exhibited stable baselines. Next, the nanoparticle suspensions were injected while Δf and ΔD were continuously monitored at the third to the 13th overtone ($n = 3-13$) for the polystyrene latex and at the third to the ninth overtone ($n = 3-9$) for the Pd-nZVI. Temperature and flow rates were kept constant throughout the duration of the experiment at 22 °C and at 100 μL/min, respectively. Each experimental condition was assessed in triplicate. The QCM-D measurements on the QDs were adopted from previously published data.[24]

Before each measurement, the QCM-D sensor crystals were cleaned in an ultrasonic bath at 100 W and at 42 kHz (model FS60, Fisher Scientific, Pittsburgh) for 15 min while immersed in 2% Hellmanex and thereafter thoroughly rinsed in deionized water, dried under N_2, and exposed to UV/ozone treatment for at least 10 min. After each measurement, the crystals, QCM-D chambers, and tubing were rinsed with 2 mL of 2% Hellmanex (Fisher Scientific) followed by 4 mL of DI water.

Conflict of Interest: The authors declare no competing financial interest.

Acknowledgment. The authors acknowledge the financial support of the Natural Sciences and Engineering Research Council of Canada (Discovery Grant to N.T. and NSERC Strategic Research Network on Bioactive Paper - SENTINEL), the CRC Program, Environment Canada, and the Ministère du Développement Économique, Innovation et Exportation (MDEIE).

Supporting Information Available: Schematic depiction of the deposited nanoparticle sizing analysis in QCM-D and representative TEM images of QDs and Pd-nZVI particles. This material is available free of charge *via* the Internet at http://pubs.acs.org.

REFERENCES AND NOTES

1. Torchilin, V. P. Multifunctional Nanocarriers. *Adv. Drug Delivery Rev.* **2006**, *58*, 1532–1555.
2. Algar, W. R.; Susumu, K.; Delehanty, J. B.; Medintz, I. L. Semiconductor Quantum Dots in Bioanalysis: Crossing the Valley of Death. *Anal. Chem.* **2011**, *83*, 8826–8837.
3. Rai, M.; Yadav, A.; Gade, A. Silver Nanoparticles as a New Generation of Antimicrobials. *Biotechnol. Adv.* **2009**, *27*, 76–83.
4. Tratnyek, P. G.; Johnson, R. L. Nanotechnologies for Environmental Cleanup. *Nano Today* **2006**, *1*, 44–48.
5. Zhang, W. Nanoscale Iron Particles for Environmental Remediation: An Overview. *J. Nanopart. Res.* **2003**, *5*, 323–332.
6. Prieto, G.; Zečević, J.; Friedrich, H.; Jong, K. P.; Jongh, P. E. Towards Stable Catalysts by Controlling Collective Properties of Supported Metal Nanoparticles. *Nat. Mater.* **2013**, *12*, 34–39.
7. Domingos, R. F.; Baalousha, M. A.; Ju-Nam, Y.; Reid, M. M.; Tufenkji, N.; Lead, J. R.; Leppard, G. G.; Wilkinson, K. J. Characterizing Manufactured Nanoparticles in the Environment: Multimethod Determination of Particle Sizes. *Environ. Sci. Technol.* **2009**, *43*, 7277–7284.
8. Hassellöv, M.; Readman, J. W.; Ranville, J. F.; Tiede, K. Nanoparticle Analysis and Characterization Methodologies in Environmental Risk Assessment of Engineered Nanoparticles. *Ecotoxicology* **2008**, *17*, 344–361.
9. Baalousha, M.; Lead, J. R. Rationalizing Nanomaterial Sizes Measured by Atomic Force Microscopy, Flow Field-Flow Fractionation, and Dynamic Light Scattering: Sample Preparation, Polydispersity, and Particle Structure. *Environ. Sci. Technol.* **2012**, *46*, 6134–6142.
10. Sapsford, K. E.; Tyner, K. M.; Dair, B. J.; Deschamps, J. R.; Medintz, I. L. Analyzing Nanomaterial Bioconjugates: A Review of Current and Emerging Purification and Characterization Techniques. *Anal. Chem.* **2011**, *83*, 4453–4488.
11. Tellechea, E.; Johannsmann, D.; Steinmetz, N. F.; Richter, R. P.; Reviakine, I. Model-Independent Analysis of QCM Data on Colloidal Particle Adsorption. *Langmuir* **2009**, *25*, 5177–5184.
12. Reviakine, I.; Johannsmann, D.; Richter, R. P. Hearing What You Cannot See and Visualizing What You Hear. *Anal. Chem.* **2011**, *23*, 8838–8848.
13. Sauerbrey, G. Verwendung Von Schwingquarzen Zur Wiigung Dunner. Schichten Und Zur Mikrowägung. *Z. Phys.* **1959**, *155*, 206–222.
14. Johannsmann, D.; Mathauer, K.; Wegner, G.; Knoll, W. Viscoelastic Properties of Thin Films Probed with a Quartz-Crystal Resonator. *Phys. Rev. B* **1992**, *46*, 7808–7815.
15. Voinova, M. V.; Jonson, M.; Kasemo, B. "Missing Mass" Effect in Biosensor's QCM Applications. *Biosens. Biolectron.* **2002**, *17*, 835–841.
16. Carton, I.; Brisson, A. R.; Richter, R. P. Label-Free Detection of Clustering of Membrane-Bound Proteins. *Anal. Chem.* **2010**, *82*, 9275–9281.
17. Bingen, P.; Wang, G.; Steinmetz, N. F.; Rodahl, M.; Richter, R. P. Solvation Effects in the Quartz Crystal Microbalance with Dissipation Monitoring Response to Biomolecular Adsorption. A Phenomenological Approach. *Anal. Chem.* **2008**, *80*, 8880–8890.
18. Johannsmann, D.; Reviakine, I.; Richter, R. P. Dissipation in Films of Adsorbed Nanospheres Studied by Quartz Crystal Microbalance (QCM). *Anal. Chem.* **2009**, *81*, 8167–8176.
19. Dultsev, F. N.; Kolosovsky, E. A. Quartz Crystal Microbalance as a Sensing Active Element for Rupture Scanning within Frequency Band. *Anal. Chim. Acta* **2011**, *687*, 75–81.
20. Chen, K. L.; Elimelech, M. Aggregation and Deposition Kinetics of Fullerene (C_{60}) Nanoparticles. *Langmuir* **2006**, *22*, 10994–11001.
21. Chen, K. L.; Elimelech, M. Interaction of Fullerene (C_{60}) Nanoparticles with Humic Acid and Alginate Coated Silica Surfaces: Measurements, Mechanisms, and Environmental Implications. *Environ. Sci. Technol.* **2008**, *42*, 7607–7614.
22. Fatisson, J.; Domingos, R. F.; Wilkinson, K. J.; Tufenkji, N. Deposition of TiO_2 Nanoparticles onto Silica Measured Using a Quartz Crystal Microbalance with Dissipation Monitoring. *Langmuir* **2009**, *9*, 6062–6069.
23. Fatisson, J.; Ghoshal, S.; Tufenkji, N. Deposition of Carboxymethylcellulose-Coated Zero-Valent Iron Nanoparticles onto Silica: Roles of Solution Chemistry and Organic Molecules. *Langmuir* **2010**, *26*, 12832–12840.
24. Quevedo, I. R.; Olsson, A. L. J.; Tufenkji, N. Deposition Kinetics of Quantum Dots and Polystyrene Latex Nanoparticles onto Alumina: Role of Water Chemistry and Particle Coating. *Environ. Sci. Technol.* **2013**, *47*, 2212–222024.
25. Reviakine, I.; Gallego, M.; Johannsmann, D.; Tellechea, E. Adsorbed Liposome Deformation Studied with Quartz Crystal Microbalance Adsorbed Liposome Deformation Studied with Quartz Crystal Microbalance. *J. Chem. Phys.* **2012**, 084702.
26. Yopps, J.; Fuerstenau, D. The Zero Point of Charge of Alpha-Alumina. *J. Colloid Sci.* **1964**, *19*, 61–71.
27. Saleh, N.; Kim, H.; Phenrat, T.; Matyjaszewski, K.; Tilton, R. D.; Lowry, G. V. Ionic Strength and Composition Affect the Mobility of Surface-Modified Fe0 Nanoparticles in Water-Saturated Sand Columns. *Environ. Sci. Technol.* **2008**, *42*, 3349–3355.
28. Johannsmann, D. Viscoelastic, Mechanical, and Dielectric Mesurements on Complex Samples with the Quartz Crystal Microbalance. *Phys. Chem. Chem. Phys.* **2008**, *10*, 4516–4534.
29. Quevedo, I. R.; Tufenkji, N. Influence of Solution Chemistry on the Deposition and Detachment Kinetics of a CdTe Quantum Dot Examined Using a Quartz Crystal Microbalance. *Environ. Sci. Technol.* **2009**, *43*, 3176–3182.
30. Elimelech, M.; Gregory, J.; Jia, X. Williams, R. A. *Particle Deposition & Aggregation*; Butterworth-Heinemann, 1995.
31. Wiesner, M. R.; Bottero, J.-Y. *Environmental Nanotechnology*; McGraw-Hill, 2007.
32. Olsson, A. L. J.; Mei, H. C.; van der Johannsmann, D.; Busscher, H. J.; Sharma, P. K. Probing Colloid-Substratum

Contact Stiffness by Acoustic Sensing in a Liquid Phase. *Anal. Chem.* **2012**, *84*, 4504–4512.
33. Phenrat, T.; Saleh, N.; Sirk, K.; Kim, H.-J.; Tilton, R. D.; Lowry, G. V. Stabilization of Aqueous Nanoscale Zerovalent Iron Dispersions by Anionic Polyelectrolytes: Adsorbed Anionic Polyelectrolyte Layer Properties and Their Effect on Aggregation and Sedimentation. *J. Nanopart. Res.* **2007**, *10*, 795–814.
34. Johannsmann, D.; Reviakine, I.; Rojas, E.; Gallego, M. Effect of Sample Heterogeneity on the Interpretation of QCM (-D) Data: Comparison of Combined Quartz Crystal Microbalance/Atomic Force Microscopy Measurements with Finite Element Method Modeling. *Anal. Chem.* **2008**, *80*, 8891–8899.
35. Quevedo, I. R.; Tufenkji, N. Mobility of Functionalized Quantum Dots and a Model Polystyrene Nanoparticle in Saturated Quartz Sand and Loamy Sand. *Environ. Sci. Technol.* **2012**, *46*, 4449–4457.